Prototype of Real-Time Orbit Service for LEO Navigation Satellite System

Guanlong Meng, Haibo Ge(✉), and Bofeng Li

College of Surveying and Geo-Informatics, Tongji University, Shanghai 200092, China
haibo_ge@tongji.edu.cn

Abstract. With continuous deployment of Low Earth Orbit (LEO) satellites and development of inter-satellite links, LEO enhanced Global Navigation Satellite System (LeGNSS) brings new opportunities for future high-precision positioning, navigation, and timing (PNT) services. Real-time precise LEO orbit is the prerequisite for real-time precise positioning. In order to provide precise real-time LEO orbit and guarantee the normal operation of LeGNSS, a prototype of real-time orbit service for LEO navigation satellite system is proposed. We evaluate the accuracy of LEO orbit, and demonstrate the system infrastructure and working principle. In addition, two real-time LEO orbit broadcasting methods are designed: (1) using LEO orbit determined by RTS products as the fitting part to predict orbit, the prediction part is fitted by ephemeris parameters, which are injected into LEO and broadcasted to users. (2) differences between LEO orbits obtained by RTS products and the broadcast ephemeris are used to generate orbit corrections and broadcasted to users. Results show that LEO near-real-time orbit achieves centimeter-level accuracy, and the fitting errors of broadcast ephemeris are smaller than 10 cm in 20-min fitting arc. Moreover, the LEO broadcast ephemeris would obtain decimeter-level accuracy orbit, while the orbit corrections method would provide users with real-time centimeter-level LEO orbit.

Keywords: LEO · Real-time processing · Precise orbit determination · Orbit fitting and prediction

1 Introduction

With the deployment of LEO constellation and the increasing demand of precise real-time positioning, LeGNSS [1] is becoming the main trend for future positioning, navigation and timing (PNT), which would provide users with high accuracy real-time positioning services, rapid convergence precise point positioning (PPP) applications and low-latency LEO data transmission. However, a prerequisite for real-time high accuracy positioning services is LEO precise orbit. Currently, orbit determination methods mainly include kinematic precise orbit determination (KPOD) and reduced-dynamic POD (RDPOD). The KPOD based on onboard receiver only uses GNSS observations to determine LEO satellite orbit, which has the advantages of low cost, easy deployment, high accuracy, global and continuous observation. In addition, the kinematic method is less computationally intensive since it introduces no dynamic force models.

C. Yang and J. Xie (Eds.): CSNC 2024, LNEE 1094, pp. 103–117, 2024.
https://doi.org/10.1007/978-981-99-6944-9_10

In the early studies of real-time orbit determination, KPOD was not widely used due to the lack of precise real-time orbit and clock products. Ashkenazi et al. [2] demonstrated that the accuracy of real-time TOPEX/POSEIDON satellite orbit could reach 1 m by using dynamic force models. Gill et al. [3] clarified that X-SAT achieved real-time orbit accuracy of 1–2 m by L1 code and phase combined observations and dynamic force models. Using SAC-C dual-frequency observations, Reichert et al. [4] obtained real-time orbit with a 3D accuracy of 1.5 m. Montenbruck and Ramos-Bosch [5] utilized GPS broadcast ephemeris to determine real-time LEO orbit with a 3D accuracy of about 0.5 m. However, the above studies all used dynamic force models, which required high computational capability and leads to latency.

With the launch of IGS-RTS [6] and the refinement of GNSS POD strategies, the accuracy of GNSS real-time orbit and clock products has been improved [7], giving opportunities for real-time KPOD. Chen et al. [8] used single-frequency observations and International GNSS Service (IGS) ultra-rapid products to obtain real-time LEO orbit with a 3D accuracy of 0.72 m. With zero-differenced and dual-frequency observations, Li et al. [9] achieved Sentinel-3A and Swarm-A centimeter-level real-time orbit determination. Wang et al. [10] utilized SSR products to obtain real-time GRACE orbit with a 3D accuracy smaller than 11 cm. As the orbit products for the potential LEO applications, broadcast ephemeris is one of the ways for users to obtain real-time LEO positions and velocities. A small eccentricity or small orbital inclination would lead to singularities in LEO broadcast ephemeris fitting. Xie et al. [11] used nonsingular parameters to eliminate the singularity caused by a small eccentricity. Meng et al. [12] considered the case of small orbit inclination and obtained a broadcast ephemeris scheme with a centimeter-level URE by simulated orbit. However, the above studies did not discuss the fitting scheme and accuracy of real-time LEO orbit. In order to provide precise real-time LEO orbit and guarantee the normal operation of LeGNSS, we propose a prototype of real-time orbit service for LEO navigation satellite system based on GNSS real-time services, and design a complete process from LEO satellite orbit determination to broadcasting LEO ephemeris and real-time corrections.

To assess the feasibility of proposed system, we carry out experiments on LEO orbit determination, real-time LEO orbit prediction and LEO broadcast ephemeris fitting. Moreover, the performance of real-time LEO orbit services is evaluated in details.

2 Real-Time LEO POD System

2.1 System Composition

Real-time LEO POD system includes monitor station, mater control station, and injection station, as shown in Fig. 1. The monitor station collects data and transmits them to the master control station. Here, LEO satellites are assumed to have the capability of transmitting big data with inter-satellite links (ISL). GNSS orbit and clock products are obtained from network. The master control station generates LEO orbit, broadcast ephemeris and real-time corrections. Broadcast ephemeris are injected to LEO satellites by the injection station, and then broadcasted to users, while real-time corrections can be broadcasted to users via internet or communication systems.

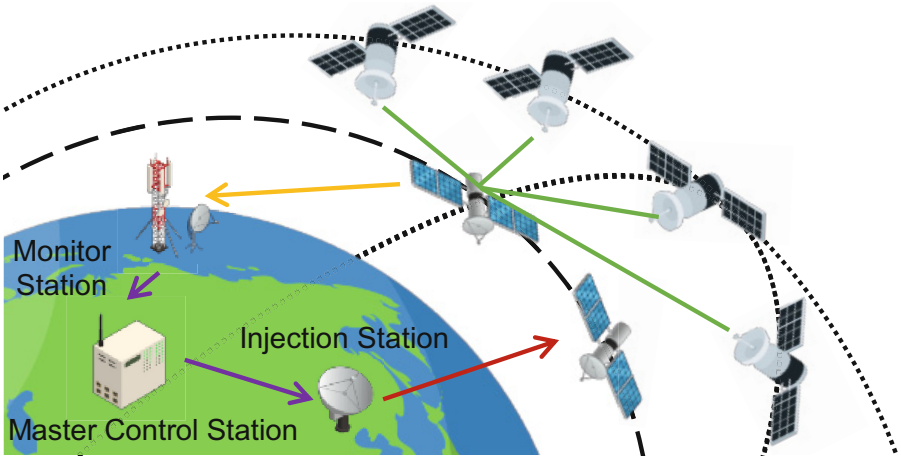

Fig. 1. Real-time LEO precise orbit service system.

2.2 System Working Principle

Figure 2 illustrates the processing flow of the real-time orbit service system in the master control station. The system includes four modules: LEO precise orbit determination module, real-time corrections generation module, real-time orbit prediction module, and LEO broadcast ephemeris fitting module. The working principle of each module is described as follows.

LEO POD Module

After data preprocessing, such as cycle slip detection and rejecting low elevation satellites, PPP is used to determine LEO orbit. The onboard code and phase observations can be expressed as

$$P_{r,j}^{s} = \rho_r^s + dt_r - dt^s + \mu_j \iota_{r,1}^s + D_{r,j} - d_j^s + \varepsilon_{P_{r,j}^s} \tag{1}$$

$$\Phi_{r,j}^{s} = \rho_r^s + dt_r - dt^s + B_{r,j} - b_j^s + \lambda_j \left(N_{r,j}^s + \varphi_{r,j} + \varphi_j^s \right) - \mu_j \iota_{r,1}^s + \varepsilon_{\Phi_{r,j}^s} \tag{2}$$

where r, s and j donate receiver, satellite and signal frequency, respectively. Since the height of LEO orbit is higher than the troposphere, the effect of tropospheric delay is not considered. dt_r And dt^s donate receiver and satellite clock, respectively. $D_{r,j}$ And $B_{r,j}$ are receiver hardware delays of code and phase, respectively. d_j^s And b_j^s are satellite hardware delays of code and phase, respectively. $\mu_j = f_1^2/f_j^2$ Represents the factor of ionospheric delay, which is used to calculate the ionospheric delay of other frequencies. $\iota_{r,1}^s$ is the f_1 frequency ionospheric delay on the oblique path. λ_j is the f_j wavelength and $N_{r,j}^s$ is the corresponding integer ambiguity. $\varphi_{r,j}$ And φ_j^s are the initial phase biases of receiver and satellite, respectively. $\varepsilon_{P_{r,j}^s}$ And $\varepsilon_{\Phi_{r,j}^s}$ are observation noise of code and phase, respectively. The remaining errors such as antenna phase center offset (PCO), antenna phase center variation (PCV), phase wind up, and relativistic effects

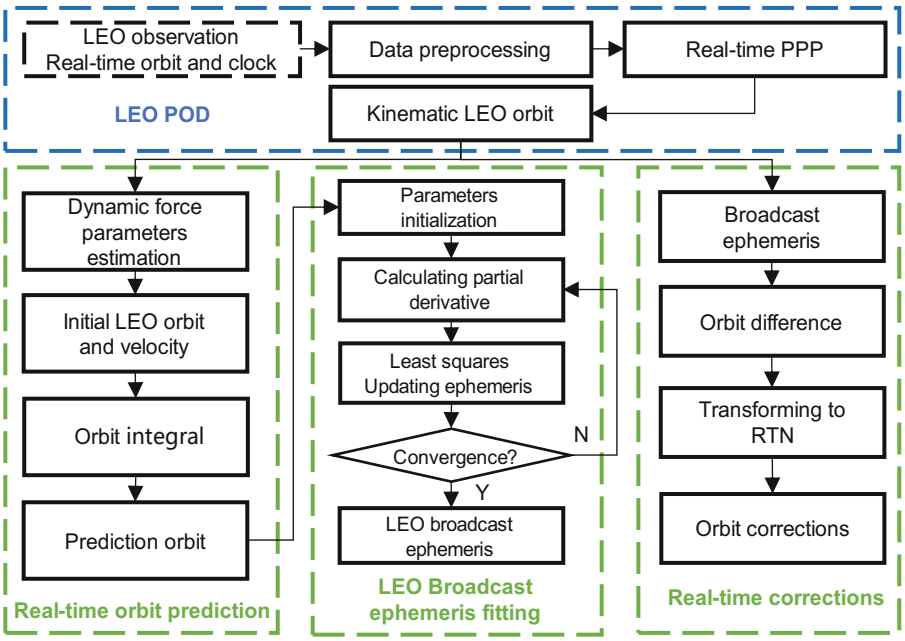

Fig. 2. Processing flowchart of the master control station.

are corrected by models. In addition, the ionosphere-free (IF) combination is used to eliminate the first-order ionospheric delay, which can be expressed as

$$P^s_{r,\mathrm{IF}} = \rho^s_r + dt_r - dt^s + D_{r,\mathrm{IF}} - d^s_{\mathrm{IF}} + \varepsilon_{\mathrm{P}^s_{r,\mathrm{IF}}} \tag{3}$$

$$\Phi^s_{r,\mathrm{IF}} = \rho^s_r + dt_r - dt^s + B_{r,\mathrm{IF}} - b^s_{\mathrm{IF}} + \lambda_{\mathrm{IF}}\left(N^s_{r,\mathrm{IF}} + \varphi_{r,\mathrm{IF}} + \varphi^s_{\mathrm{IF}}\right) + \varepsilon_{\Phi^s_{r,\mathrm{IF}}} \tag{4}$$

Real-time Corrections Generation Module

Real-time orbit correction is generally expressed in the satellite coordinate system. Firstly, making difference between the real-time and broadcast ephemeris orbits. Then, the orbit corrections in along-track, cross-track, and radial components are obtained by converting the orbit difference to satellite coordinate system. The above steps can be expressed as follows.

$$\begin{bmatrix} \delta x \\ \delta y \\ \delta z \end{bmatrix} = \begin{bmatrix} x_b \\ y_b \\ z_b \end{bmatrix} - \begin{bmatrix} x_p \\ y_p \\ z_p \end{bmatrix} \tag{5}$$

where $\begin{bmatrix} x_b & y_b & z_b \end{bmatrix}^T$ and $\begin{bmatrix} x_p & y_p & z_p \end{bmatrix}^T$ are the vector of broadcast ephemeris orbit and precise LEO orbit, respectively. The satellite positions $\boldsymbol{r}$ and velocities $\dot{\boldsymbol{r}}$ are calculated by the broadcast ephemeris to create the rotation matrix $\boldsymbol{R}$

$$\boldsymbol{R} = \left[\frac{\dot{\boldsymbol{r}}}{|\dot{\boldsymbol{r}}|} \times \frac{\boldsymbol{r}\times\dot{\boldsymbol{r}}}{|\boldsymbol{r}\times\dot{\boldsymbol{r}}|} \quad \frac{\dot{\boldsymbol{r}}}{|\dot{\boldsymbol{r}}|} \quad \frac{\boldsymbol{r}\times\dot{\boldsymbol{r}}}{|\boldsymbol{r}\times\dot{\boldsymbol{r}}|} \right] \tag{6}$$

According to the rotation matrix $\boldsymbol{R}$, real-time orbit corrections are transformed from the earth-fixed coordinate system to the satellite coordinate system

$$\begin{bmatrix} \delta r \\ \delta t \\ \delta n \end{bmatrix} = \boldsymbol{R}^{-1} \begin{bmatrix} \delta x \\ \delta y \\ \delta z \end{bmatrix} \tag{7}$$

Real-Time Orbit Prediction Module

Due to complicated perturbing dynamic terms of LEO, simple fitting methods, such as Lagrange and Chebyshev interpolation, cannot meet the requirement of prediction accuracy for long arc [13]. Dynamic force models take the LEO force information into account, which achieve high precision in predicting orbit and obtain the LEO position and velocity at any time by orbit integration [14, 15]. Therefore, dynamic force models are used to fit and predict real-time LEO orbit in this study. The motion equation of a LEO satellite can be expressed as [16]

$$\ddot{\boldsymbol{r}} = -GM_e \frac{\boldsymbol{r}}{r^3} + f(t, \boldsymbol{r}, \dot{\boldsymbol{r}}, \boldsymbol{p}) + \boldsymbol{T} \cdot \boldsymbol{a}_e \tag{8}$$

where $\boldsymbol{r}, \dot{\boldsymbol{r}}$, and $\ddot{\boldsymbol{r}}$ donate the position, velocity, and acceleration of LEO, respectively. GM_e is the Earth's gravitational constant. $\boldsymbol{p}$ is the vector of dynamic force model parameters to be estimated. $\boldsymbol{T}$ is the transformation matrix from the ECEF to the ECI. $\boldsymbol{a}_e = [a_a, a_c, a_r]^T$ is the vector of empirical force accelerations in along-track, cross-track and radial directions, which is used to absorb the unmodeled forces. Using the LEO orbit from t_1 to t_n, the dynamic force parameters are estimated as follows.

$$\begin{bmatrix} \boldsymbol{r}_{t_1} - \boldsymbol{r}^0_{t_1} \\ \boldsymbol{r}_{t_2} - \boldsymbol{r}^0_{t_2} \\ \vdots \\ \boldsymbol{r}_n - \boldsymbol{r}^0_{t_n} \end{bmatrix} = \begin{bmatrix} \boldsymbol{\Phi}(t_1, t_0) \\ \boldsymbol{\Phi}(t_2, t_0) \\ \vdots \\ \boldsymbol{\Phi}(t_n, t_0) \end{bmatrix} \begin{bmatrix} \Delta \boldsymbol{r}_0 \\ \Delta \dot{\boldsymbol{r}}_0 \\ \Delta \boldsymbol{p}_0 \\ \Delta \boldsymbol{a}_{e_0} \end{bmatrix} \tag{9}$$

where $\boldsymbol{r}^0_{t_i}$ is the LEO position determined by KPOD, and r_{t_i} is the LEO position at t_i obtained by the orbit integral. $\Delta \boldsymbol{r}_0$, $\Delta \dot{\boldsymbol{r}}_0$, $\Delta \boldsymbol{p}_0$ and $\Delta \boldsymbol{a}_{e_0}$ are the corrections of position, velocity, dynamic force parameters and empirical force accelerations at t_0, respectively. $\boldsymbol{\Phi}(t_i, t_0)$ is the status transition matrix from t_i to t_0, which is expressed as

$$\boldsymbol{\Phi}(t_i, t_0) = \begin{bmatrix} \frac{\partial \boldsymbol{r}_i}{\partial \boldsymbol{r}_0} & \frac{\partial \boldsymbol{r}_i}{\partial \dot{\boldsymbol{r}}_0} & \frac{\partial \boldsymbol{r}_i}{\partial \boldsymbol{p}_0} & \frac{\partial \boldsymbol{r}_i}{\partial \boldsymbol{a}_{e_0}} \end{bmatrix} \tag{10}$$

LEO Broadcast Ephemeris Fitting Module

In the broadcast ephemeris fitting, using the partial derivative of each parameter, the linear equation can be written as

$$\boldsymbol{Y} = \boldsymbol{F}_0 + \frac{\partial \boldsymbol{Y}}{\partial \sqrt{a}} \partial \sqrt{a} + \frac{\partial \boldsymbol{Y}}{\partial i} \partial i + \cdots + \frac{\partial \boldsymbol{Y}}{\partial Cuc2} \partial Cuc2 \tag{11}$$

where $\boldsymbol{Y}$ is the real-time LEO position and $\boldsymbol{F}_0$ is the approximate position obtained by user algorithm with the initial parameters. $\frac{\partial \boldsymbol{Y}}{\partial \sqrt{a}}, \frac{\partial \boldsymbol{Y}}{\partial i}, \ldots, \frac{\partial \boldsymbol{Y}}{\partial Cuc2}$ are the partial derivatives of each parameter and $\partial\sqrt{a}, \partial i, \ldots, \partial Cuc2$ are corresponding parameter corrections. According to Eq. (11), the error equation can be express as

$$\begin{bmatrix} \boldsymbol{V}_{X_i} \\ \boldsymbol{V}_{Y_i} \\ \boldsymbol{V}_{Z_i} \end{bmatrix} = \begin{bmatrix} \frac{\partial \boldsymbol{X}_i}{\partial \sqrt{a}} & \frac{\partial \boldsymbol{X}_i}{\partial i} & \cdots & \frac{\partial \boldsymbol{X}_i}{\partial Cuc2} \\ \frac{\partial \boldsymbol{Y}_i}{\partial \sqrt{a}} & \frac{\partial \boldsymbol{Y}_i}{\partial i} & \cdots & \frac{\partial \boldsymbol{Y}_i}{\partial Cuc2} \\ \frac{\partial \boldsymbol{Z}_i}{\partial \sqrt{a}} & \frac{\partial \boldsymbol{Z}_i}{\partial i} & \cdots & \frac{\partial \boldsymbol{Z}_i}{\partial Cuc2} \end{bmatrix} \begin{bmatrix} \partial\sqrt{a} \\ \partial i \\ \vdots \\ \partial Cuc2 \end{bmatrix} + \begin{bmatrix} \boldsymbol{X}_{i0} - \boldsymbol{X}_i \\ \boldsymbol{Y}_{i0} - \boldsymbol{Y}_i \\ \boldsymbol{Z}_{i0} - \boldsymbol{Z}_i \end{bmatrix} \tag{12}$$

The broadcast ephemeris parameters are estimated using the iterative least squares

$$\Delta \boldsymbol{X} = \left(\boldsymbol{A}^T \boldsymbol{A}\right)^{-1} \boldsymbol{A}^T \boldsymbol{l} \tag{13}$$

$$\boldsymbol{X} = \boldsymbol{X}_0 + \Delta \boldsymbol{X}_1 + \Delta \boldsymbol{X}_2 + \cdots + \Delta \boldsymbol{X}_n \tag{14}$$

where $\boldsymbol{X}_0$ is the initial ephemeris parameter vector and $\Delta \boldsymbol{X}_n$ is the vector of corrections for the nth iteration.

3 Data Set and Processing Strategies

3.1 Data Set

We use GRACE-FO Level-1B onboard observations in January 2019 to obtain kinematic orbit and use the reduced-dynamic orbits provided by the Jet Propulsion Laboratory (JPL) to assess the accuracy of near-real-time LEO orbit determination. The sampling intervals of the onboard observation and reduced-dynamic orbit are 10s and 1s, respectively, both of which can be downloaded from the Physical Oceanography DAAC (PO.DAAC) website (https://podaac-tools.jpl.nasa.gov/). To obtain the near-real-time orbit, the Centre National D'Etudes Spatiales (CNES) real-time orbit and clock products (CNT) with a sampling of 5s and latency of 8s are used, which can be downloaded from the PPP-Wizard website (http://www.ppp-wizard.net/products/).

3.2 Processing Strategies of LEO POD

Processing strategies of LEO kinematic orbit determination are shown in Table 1. Undifferenced IF observations of GPS code and phase are used. Melbourne-Wübbena (MW) and Geometry-Free (GF) combination are employed in cycle slip detection. GPS antenna phase center errors are corrected with the IGS14.atx file, which can be downloaded from the IGS website (https://files.igs.org/pub/station/general/). GRACE-FO PCO are corrected by the Level-1B phase center offset product VGN1B and the rotation quaternions product SCA1B. Since GRACE-FO lacks priori PCV information and related products, we use the post-processing phase residuals to build PCV models with a grid size of 5° × 5°.

Table 1. Processing strategy of KPOD for LEO.

Items	Description
Observation model	Undifferenced IF code and phase
Stochastic model	Elevation dependent model
Elevation cutoff	10°
Sampling rate	10s
Estimation method	Extended Kalman Filter
GPS orbits and clocks	CNES real-time products
Cycle slip detection	MW and GF combination
LEO positions	White noise
Phase ambiguities	Estimated as float constant
Phase wind up	Model correction [17]
GPS PCO/PCV	IGS14.atx
LEO PCO	VGN1B + SCA1B
LEO PCV	Residual method PCV model

3.3 Processing Strategies of Dynamic Orbit Prediction

Prediction accuracy is related to the dynamic force models. The dynamic force models and the parameters to be estimated for predicting GRACE-FO orbit are listed in Table 2. Atmosphere drag and empirical force parameters are estimated every one cycle per revolution, which is about 90 min.

3.4 Processing Strategies of Broadcast Ephemeris Fitting

The altitude of GRACE-FO is 400–500 km and the orbit eccentricity is about 0.005. The orbital period (T) of GRACE-FO is about 94.8 min. To eliminate the singularity caused by a small eccentricity, nonsingular elements ($\sqrt{a}$, e_x, e_y, λ, i, Ω) are used to replace the classical Kepler 6 elements. The transformation can be expressed as

$$\begin{cases} e_x = e \cdot \cos(\omega) \\ e_y = e \cdot \sin(\omega) \\ \lambda = \omega + M_0 \end{cases} \tag{15}$$

where e, ω, and M_0 are eccentricity, argument of perigee and mean anomaly, respectively. In order to assess the characteristics of GRACE-FO orbit, the variations of nonsingular elements are analyzed. Figure 3 presents the time series and amplitude spectrum of the nonsingular elements during one day. It can be seen that the RAAN (Ω) shows mainly a linear variation, while the other elements show periodic variations in the form of harmonics. The short period of the semi-axis (a) and orbital inclination (i) is about $T/2$. The elements e_x and e_y exhibit a short period of about $T/3$, and the short period of

Table 2. Force models and estimated parameters.

Item	Description
Force models	
Earth gravity	EGM2008(120 × 120) [18]
Solid earth tide	IERS 2010 [19]
Ocean tide	IERS 2010 [19]
Solar radiation	Macro model [20]
N-body	JPL DE405 [21]
Atmosphere drag	DTM94 [22]
Estimated parameters	
LEO orbits	Initial positions and velocities
Atmosphere drag	A scale factor estimated every one cycle per revolution (90 min)
Empirical force	Ca, Sa, Cc, and Sc for along- and cross-track components (sine/cosine) every one cycle per revolution

larger amplitude for the element λ is $T/2$. In order to fit the LEO orbit accurately, the effects of the above short-periodic perturbation terms need to be considered. Therefore, based on the GPS LNAV parameters, we simulate the LEO perturbation by adding different additional parameters to develop an applicable broadcast ephemeris scheme for real-time LEO orbit. The additional parameters are listed in Table 3, including short-periodic corrections and secular corrections. Short-periodic corrections contain the first- and third-order amplitude of sine and cosine harmonic correction term to the angle of inclination i, the orbit radius r and the argument of latitude u. Secular corrections contain the change rate of the semi-major axis a and the mean motion n.

4 Results and Analysis

4.1 Analysis of Near-Real-Time Kinematic Orbit Accuracy

Figure 4 shows the position errors of GRACE-FO near-real-time kinematic orbit on January 27, 2019. It can be found that the convergence time is needed at the beginning of the orbit determination. During this period, the orbit errors fluctuate largely, and the results are of low accuracy. After convergence, the position errors in along-track, cross-track and radial components are generally smaller than 10 cm.

In order to evaluate the accuracy of near-real-time LEO orbit, we use the onboard observation from January 1 to 30, 2019 to obtain GRACE-FO orbits. Table 4 shows the Root Mean Square Error (RMSE) of GRACE-FO kinematic orbit. It can be found that the RMSE of GRACE-C and GRACE-D kinematic orbit are smaller than 6 cm in along-track, cross-track, and radial directions. The 3D RMSE are smaller than 10 cm, which means that the near-real-time orbit reaches centimeter-level accuracy.

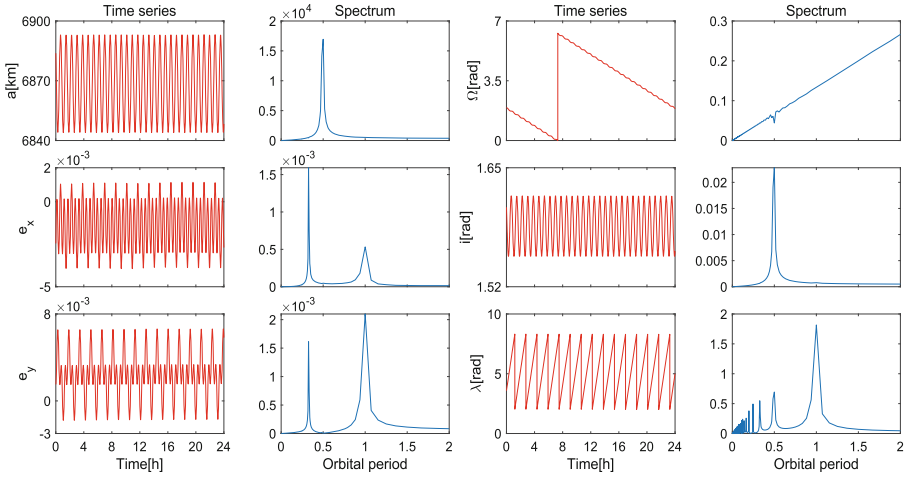

Fig. 3. Time series (red) and amplitude spectrum (blue) of 6 orbit nonsingular elements for GRACE-FO.

Table 3. Additional parameters.

Description	Parameters
Short-periodic correction	$Cus1$, $Cuc1$, $Crs1$, $Crc1$, $Cis1$, $Cic1$ $Cus3$, $Cuc3$, $Crs3$, $Crc3$, $Cis3$, $Cic3$
Secular correction	$\dot{a}$, $\dot{n}$

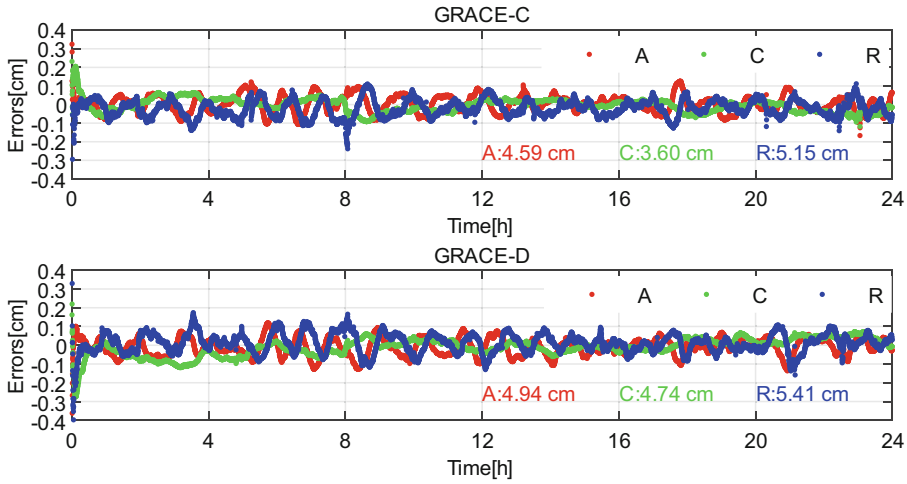

Fig. 4. GRACE-FO near-real-time kinematic orbit errors.

Table 4. RMSE of GRACE-FO near-real-time kinematic orbit.

RMSE/cm	Along-track	Cross-track	Radial	3D
GRACE-C	5.47	3.95	5.82	8.91
GRACE-D	5.33	4.51	5.81	9.08

4.2 Analysis of Dynamic Prediction Orbit Accuracy

In order to obtain real-time orbit, dynamic force models are used to fit and predict the near-real-time orbit. The fitting and prediction arcs are 24 h and 30 min, respectively. Figure 5 presents the prediction errors of 30-min prediction arc compared with the reference orbit in along-track, cross-track and radial components. The prediction errors of along-track and radial components varies within 5 cm.

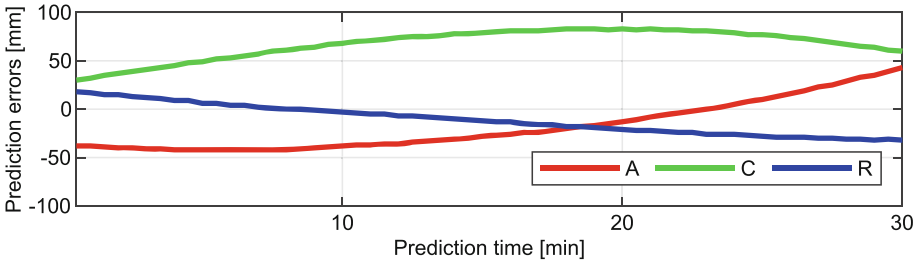

Fig. 5. Prediction errors of near-real-time kinematic orbit in along-track (red), cross-track (green) and radial (blue) components.

Table 5 lists the RMSE of the GRACE-FO real-time prediction orbit errors for DOY001~030 in 2019. For 20-min prediction time, the prediction accuracy is better than 10 cm for GRACE-C and GRACE-D in along-track, cross-track and radial directions, with the smallest error in cross-track direction and large errors in radial and along-track directions. For the 30-min prediction arc, the along-track error is larger than 10 cm, while the errors in radial and cross-track directions are less than 10 cm.

Table 5. RMSE of GRACE-FO real-time prediction orbit.

	Prediction arc (min)	Along-track/cm	Cross-track/cm	Radial/cm
GRACE-C	20	7.78	4.11	5.18
	30	11.76	4.60	8.39
GRACE-D	20	6.29	2.13	6.25
	30	10.83	2.14	7.56

4.3 Analysis of LEO Broadcast Ephemeris Accuracy

Table 6 shows the fitting UREs and the corresponding additional parameters for 16-, 18-, 20-, 22-, and 24-parameter broadcast ephemeris schemes in 20- and 30-min fitting arcs. Compared with the 16-parameter scheme, $\dot{a}$ and $\dot{n}$ in the 18-parameter scheme improve the fitting accuracy in along-track and radial directions significantly. The first- and third-order amplitudes of harmonic correction terms to the orbit radius (r) and the argument of latitude (u) would fit along-track direction better than $\dot{a}$ and $\dot{n}$. Combining the additional parameters in 18-parameter scheme, the 20-parameter scheme containing $\dot{a}$ and $\dot{n}$ has smaller fitting errors for along-track direction, while the radial fitting accuracy is better for the scheme without $\dot{a}$ and $\dot{n}$. The fitting errors of 22-paramenter schemes are comparable in the along-track, cross-track, and radial components, and the UREs are about 5 cm for the 20-min fitting arc. In order to improve the fitting accuracy, the amplitudes of harmonic correction term to the orbital inclination *Cis*3 and *Cic*3 are added to the 22-parameter scheme. Compared with the 22-parameter, the cross-track fitting accuracy of the 24-parameter scheme is significantly improved by about 1 cm, and the URE is smaller than 4 cm.

Table 6. RMSE of fitting errors for GRACE-D real-time prediction orbit.

Parameter number	Additional parameters	20 min (cm)				30 min (cm)			
		A	C	R	URE	A	C	R	URE
16	–	37.54	5.98	19.89	25.79	97.71	21.67	67.59	70.22
18	$\dot{a}$, $\dot{n}$	18.64	5.74	11.4	13.40	54.79	21.33	34.53	40.43
	*Cus*1, *Cuc*1	7.96	5.62	18.66	10.01	24.28	21.18	63.65	33.74
	*Crs*1, *Crc*1	7.97	5.62	18.67	10.02	24.27	21.16	63.61	33.72
	*Cus*3, *Cuc*3	7.48	5.61	18.64	9.85	21.54	21.16	63.76	32.99
	*Crs*3, *Crc*3	8.19	5.6	11.29	7.93	26.08	21.14	32.07	25.40
20	$\dot{a}$, $\dot{n}$, *Cus*3, *Cuc*3	4.9	5.55	11.01	6.62	13.91	20.94	32.56	21.13
	$\dot{a}$, $\dot{n}$, *Crs*3, *Crc*3	5.4	5.56	7.73	5.94	15.37	20.88	19.33	18.51
	*Cus*1, *Cuc*1, *Crs*3, *Crc*3	8.03	5.62	5.58	6.71	24.30	21.18	19.98	22.32
	*Crs*1, *Crc*1, *Cus*3, *Cuc*3	8.81	5.63	5.66	7.12	26.80	21.24	20.42	23.56
22	$\dot{a}$, $\dot{n}$, *Cus*1, *Cuc*1, *Crs*3, *Crc*3	5.11	5.55	4.1	5.14	14.78	20.94	14.72	17.57
	$\dot{a}$, $\dot{n}$, *Crs*1, *Crc*1, *Cus*3, *Cuc*3	5.62	5.55	4.17	5.36	16.06	20.95	14.87	18.06
24	$\dot{a}$, $\dot{n}$, *Cus*1, *Cuc*1, *Crs*3, *Crc*3, *Cis*3, *Cic*3	5.13	1.68	3.64	3.79	14.77	7.55	12.92	11.95

Fitting results of GRACE-D are shown in Fig. 6, where 16-parameter scheme includes $\left(t_{oe}, \sqrt{a}, e_x, e_y, \lambda, i, \Omega, \Delta n, \dot{\Omega}, \dot{i}, Cus2, Cuc2, Cis2, Cic2, Crs2, Crc2\right)$, 18-,

20-, 22- and 24-schemes are the smallest URE solutions in Table 6. Generally, the URE of 20-min fitting arc is smaller than that of 30-min fitting arc with the same elements. With increasing number of parameters, the fitting accuracy of broadcast ephemeris is improved. The fitting accuracies of the 18-, 20-, 22- and 24-parameter schemes reach centimeter level for 20-min fitting arc. In order to provide high-accuracy LEO broadcast ephemeris, the 24-parameter scheme is recommended.

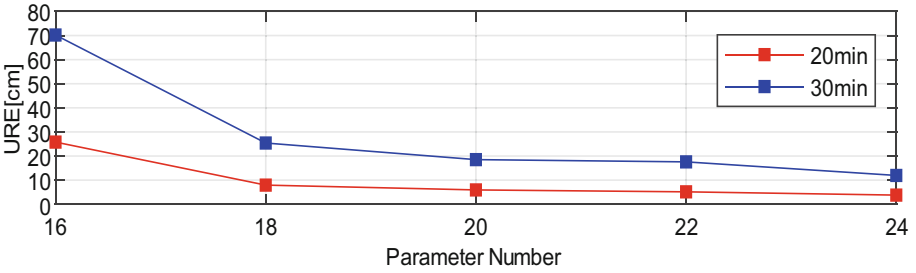

Fig. 6. Fitting UREs of GRACE-FO orbit for 16-, 18-, 20-, 22-, and 24-parameter schemes with 20- and 30-fitting arcs.

However, the above results do not consider the errors of orbit determination and prediction. To assess the accuracy of LEO broadcast ephemeris, the real-time prediction orbit broadcast ephemeris is compared with the post-processing reference orbit from January 1 to 30, 2019. Figure 7 shows the daily RMSEs of the 24-parameter ephemeris in along-track, cross-track, and radial directions. It can be found that the errors of GRACE-C and GRACE-D broadcast ephemeris are about 10 cm in along-track and radial directions, and generally smaller than 5 cm in cross-track direction for 20-min prediction arc.

Figure 8 shows the daily UREs of GRACE-FO real-time broadcast ephemeris for DOY001~030 in 2019. The average UREs of GRACE-C and GRACE-D are 12.31 cm and 10.42 cm, respectively. The LEO real-time broadcast ephemeris accuracy is near centimeter-level. With real-time corrections, the real-time LEO orbit obtained by 20-min broadcast ephemeris is restored to the real-time prediction orbit, which is of a centimeter-level accuracy in along-track, cross-track and radial components.

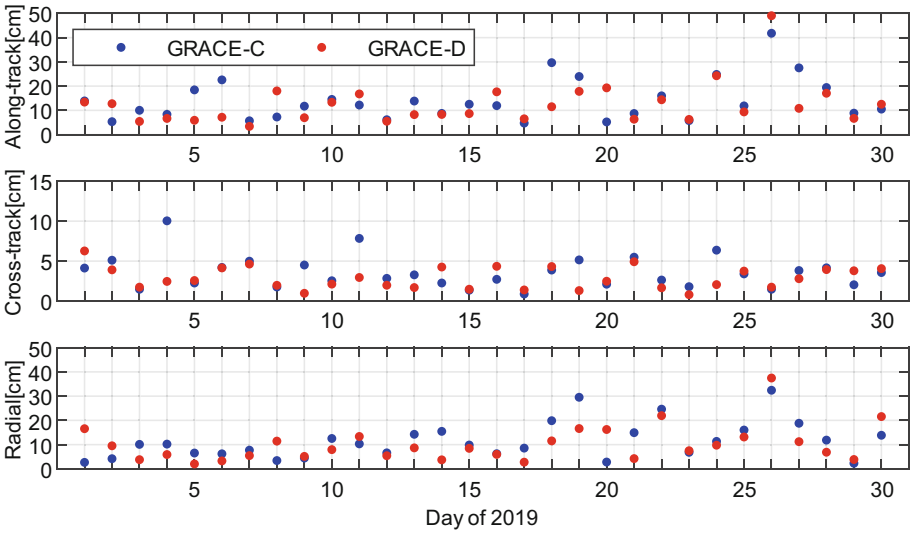

Fig. 7. Daily RMSEs of broadcast ephemeris for GRACE-C(blue) and GRACE-D(red) real-time prediction orbit in along-track(up), cross-track(middle) and radial(bottom) components.

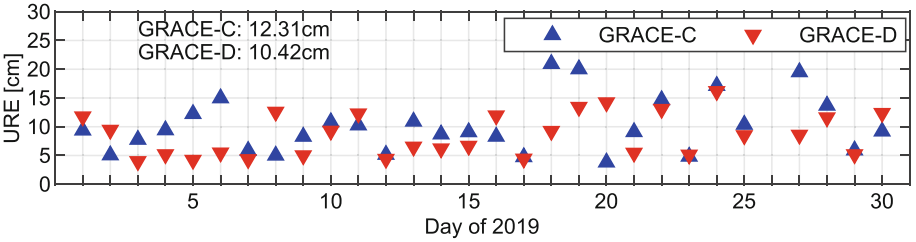

Fig. 8. Daily UREs of broadcast ephemeris for GRACE-C(blue) and GRACE-D (red) real-time prediction orbit.

5 Conclusion

In this paper, a prototype of real-time LEO orbit service system is proposed, the working principle and system process are elaborated, and the system feasibility is demonstrated by experiments. LEO orbit determination, prediction and LEO broadcast ephemeris fitting are carried out to investigate the performance of real-time orbit services for LEO satellite navigation system.

Results show that near-real-time LEO kinematic orbit can reach centimeter-level accuracy. The prediction errors in along-track, cross-track, and radial directions are centimeter-level for 20-min LEO near-real-time kinematic orbit prediction using dynamical force models, while the prediction errors increase to decimeter-level accuracy for 30-min prediction arc. Compared with the prediction orbit, the 24-parameter broadcast ephemeris scheme would achieve URE smaller than 5 cm for 20-min fitting arc, while it is near centimeter-level compared with the post-processing orbit.

In summary, the proposed real-time LEO satellite orbit service system would obtain near-real-time LEO orbit with a 3D accuracy smaller than 10cm, and provide users with centimeter to decimeter-level real-time LEO orbits by LEO broadcast ephemeris. Moreover, the service system would provide real-time centimeter-level orbits by using the real-time corrections.

Acknowledgments. This work is supported by the National Natural Science Funds of China [42104013, 42225401], Natural Science Funds of Shanghai [21ZR1465600], the Innovation Program of Shanghai Municipal Education Commission [2021-01-07–00-07-E00095], the Program of Shanghai Academic Research Leader [20XD1423800], the Fundamental Research Funds for the Central Universities, and the Scientific and Technological Innovation Plan from Shanghai Science and Technology Committee (21511103902, 22511103003).

References

1. Ge H et al (2022) LEO Enhanced Global Navigation Satellite System (LeGNSS): progress, opportunities, and challenges. Geo-spatial Inf Sci 25(1):1–13. https://doi.org/10.1080/10095020.2021.1978277
2. Ashkenazi V, Chen W, Hill CJ, Moore T, Stanton D, Fortune D, Shave N (1997) Real-time autonomous orbit determination of LEO satellites using GPS. In: Proceedings of the 10th international technical meeting of the satellite division of the institute of navigation (ION GPS 1997), pp 755–761. Kansas City, MO
3. Gill E, Montenbruck O, Arichandran K, Tan SH, Bretschneider (2004) High-precision onboard orbit determination for small satellites—the GPS-based XNS on X-SAT. In the 6th symposium on small satellites systems and services, La Rochelle, France
4. Reichert A, Meehan T, Munson T (2002) Toward decimeter-level real-time orbit determination: a demonstration using the SAC-C and CHAMP spacecraft. In: Proceedings of the 15th international technical meeting of the satellite division of the institute of navigation (ION GPS 2002). Portland, OR, pp 1996–2003
5. Montenbruck O, Ramos-Bosch P (2008) Precision real-time navigation of LEO satellites using global positioning system measurements. GPS Solutions 12(3):187–198. https://doi.org/10.1007/s10291-007-0080-x
6. Caissy M, Agrotis L, Weber G, Pajares M, Hugentobler U (2012) The international GNSS real-time service. GPS World 23:52–58
7. Li B, Ge H, Bu Y, Zheng Y, Yuan L (2022) Comprehensive assessment of real-time precise products from IGS analysis centers. Satell Navig 3(1):12. https://doi.org/10.1186/s43020-022-00074-2
8. Chen P, Zhang J, Sun X (2017) Real-time kinematic positioning of LEO satellites using a single-frequency GPS receiver. GPS Solutions 21(3):973–984. https://doi.org/10.1007/s10291-016-0586-1
9. Li X, Wu J, Zhang K, Li X, Xiong Y, Zhang Q (2019) Real-time kinematic precise orbit determination for LEO satellites using zero-differenced ambiguity resolution. Remote Sens 11(23):2815. https://doi.org/10.3390/rs11232815
10. Wang Z et al (2022) Comparison of the real-time precise orbit determination for LEO between kinematic and reduced-dynamic modes. Measurement 187:110224. https://doi.org/10.1016/j.measurement.2021.110224
11. Xie X, Geng T, Zhao Q, Liu X, Zhang Q, Liu J (2018) Design and validation of broadcast ephemeris for low earth orbit satellites. GPS Solutions 22(2):54. https://doi.org/10.1007/s10291-018-0719-9

12. Meng L, Chen J, Wang J, Zhang Y (2021) Broadcast ephemerides for LEO augmentation satellites based on nonsingular elements. GPS Solutions 25(4):129. https://doi.org/10.1007/s10291-021-01162-7
13. Zhang R, Liu G (2008) Discussion on orbit fitting and orbit forecasting of low earth orbit satellites. J Geodesy Geodyn 4:15–120 (Ch)
14. Ge H, Li B, Ge M, Nie L, Schuh H (2020) Improving low earth orbit (LEO) prediction with accelerometer data. Remote Sens 12(10):1599. https://doi.org/10.3390/rs12101599
15. Wang K, El-Mowafy A, Yang X (2022) URE and URA for predicted LEO satellite orbits at different altitudes. Adv Space Res 70(8):2412–2423. https://doi.org/10.1016/j.asr.2022.08.039
16. Jäggi A, Hugentobler U, Beutler G (2006) Pseudo-stochastic orbit modeling techniques for low-earth orbiters. J Geodesy 80(1):47–60. https://doi.org/10.1007/s00190-006-0029-9
17. Wu J, Wu S, Hajj G, Bertiger W, Lichten S (1992) Effects of antenna orientation on GPS carrier phase. Manuscr Geodaet 18(2):91–98
18. Pavlis NK, Holmes SA, Kenyon SC, Factor JK (2008) The EGM2008 global gravitational model. In: AGU fall meeting abstracts
19. Petit G, Luzum B (2010) IERS conventions (2010). Technical Reports Defense Technical Information Center Document 36:180
20. Bettadpur S (2012) GRACE Product Specification Document. CSR-GR-03-02, v4.6; Center for Space Research, University of Texas at Austin: Austin, TX, USA
21. Berger C, Biancale R, Ill M, Barlier F (1998) Improvement of the empirical thermospheric model DTM: DTM94—a comparative review of various temporal variations and prospects in space geodesy applications. J Geodesy 72(3):161–178. https://doi.org/10.1007/s001900050158
22. Standish EM (1998) JPL Planetary and Lunar Ephemerides, DE405/LE405,JPL IOM 312.F-98-048